Icarus **142**, 56–62 (1999)
Article ID icar.1999.6209, available online at http://www.idealibrary.com on IDEAL®

A Laboratory Impact Study of Simulated Edgeworth–Kuiper Belt Objects

Eileen V. Ryan,[1] Donald R. Davis, and Ian Giblin

Planetary Science Institute, 620 North Sixth Avenue, Tucson, Arizona 85705
E-mail: eryan@physics.nmhu.edu

Received October 22, 1998; revised June 24, 1999

This paper reports on a series of laboratory impact experiments designed to provide basic data on how simulated Edgeworth–Kuiper belt objects (EKOs) fragment in an impact event. In September–October 1997 we carried out 20 low-velocity airgun shots at the Ames Vertical Gun Range into porous and homogeneous ice spheres using aluminum, fractured ice, and solid ice projectiles. We found that the porous ice targets behaved as strongly as solid ice in collision. Energy is apparently well dissipated by the void spaces within the target, such that these fragile ice structures respond as if they were strong in impacts. Therefore, it would appear that if EKOs are porous, they are not collisionally weak.

Also, our data show that collisional outcomes for low-velocity impacts into ice targets depend on the type of projectile used as well as the properties of the target. We observed that the degree of fragmentation for a given type of target increases as the strength of the projectile increases. Aluminum projectiles are far more damaging to the target at the same collisional energy than are solid ice projectiles, which, in turn, are more damaging than fractured ice projectiles. One possible explanation for this behavior is the variable depth of penetration of the projectile for the different cases—stronger projectiles penetrate more deeply and couple more energy into the target than do weak projectiles. Based on this, if we assume that there has not been significant heating or differentiation in the Edgeworth–Kuiper (E–K) belt, the most applicable impact strength for the low-velocity E–K belt collisions is likely to be that derived from similar target/projectile materials impacting each other. The laboratory data from this analysis indicate that a value for impact strength $>5 \times 10^5$ erg/cm^3 is appropriate for porous ice targets impacted with solid/porous ice projectiles.

Key Words: **Kuiper belt objects; impact processes; collisional physics.**

INTRODUCTION

Since the end of the accretion phase of the Solar System approximately 4.5 Byr ago, three distinct heliocentric regions are believed to have undergone significant collisional evolution. These are the main asteroid belt (Davis *et al.* 1989), the Trojan swarms (Marzari *et al*. 1997), and the recently discovered population of small bodies orbiting at Pluto's distance and beyond, a region collectively referred to as the Edgeworth–Kuiper (E–K) belt. In the asteroid belt, collisions occur frequently on the astronomical timescale, and the same is true of the E–K belt (Stern 1995, 1996; Farinella and Davis 1996). The E–K belt is strongly depleted in mass relative to the Uranus–Neptune zone, a condition which almost certainly did not exist during the accretion phase of the formation of Edgeworth–Kuiper objects (EKOs). Otherwise, the timescale for growing a body the size of 1992 QB_1—the first identified E–K belt object (Jewitt and Luu 1993)—exceeds the age of the Solar System. Recently, Stern and Colwell (1997) suggested that collisions may have ground down >90% of the mass of the primordial E–K belt, and this mass was subsequently removed by radiation forces, similar to one mechanism proposed for the asteroid zone. Also, Farinella and Davis (1996) argued that most E–K objects smaller than about 50 km in diameter are collisionally derived fragments rather than primordial objects from the formative era of the Solar System.

Work to date on the formation and evolution of EKOs is predicated on the assumption that they have a collisional response similar to that of asteroids. Yet, there are major differences between these two populations. Among the main belt asteroids, typically consisting of rock in which the speed of sound is 2–4 km/s, the mean impact speed is 5.8 km/s and these are generally hypervelocity collisions. The mean collision speed in the E–K belt is less than ∼1 km/s (Stern 1996, Davis and Farinella 1997). The speed of sound in solid ice is ∼1.3 km/s, and although we have no data on the speed of sound in our porous targets, we think (based upon the minimum path which must be traveled by the sound wave through the porous ice structure) that this is unlikely to be reduced by as much as a factor of 4. Collisions therefore occur not as hypervelocity impacts, as is the case with asteroids, but in the subsonic regime. Many of the assumptions which appear to be valid for hypervelocity impacts, such as the point source approximation (Holsapple 1993), do not apply at lower velocities and are therefore probably not relevant to E–K belt collisions. Iijima *et al*. (1995) found a significant variation in cratering efficiency with projectile type for low-velocity cratering experiments in ice. Furthermore, EKOs are thought to consist primarily of water ice and silicates, the latter dominantly in the form of dust, and may have a high degree of porosity.

[1] Also at New Mexico Highlands University, Las Vegas, NM 87701.

0019-1035/99 $30.00

TABLE I
Experiment Results

Exp. #	Target type	Projectile type	Target mass (g)	Projectile mass (g)	Target density (g/cm^3)	Impact speed (m/s)	Energy/mass (erg/g)	f_l
970928	Crushed ice	Broken ice	715.	22.0	0.67	277.8	9.0×10^6	0.36
970929	Crushed ice	Broken ice	500.	24.0	0.69	287.0	1.7×10^7	0.12
971004	Crushed ice	Broken ice	881.	24.2	0.56	256.7	8.4×10^6	0.08
971006	Crushed ice	Broken ice	926.	24.6	0.64	175.0	3.4×10^6	0.97
971008	Crushed ice	Broken ice	1056.	24.0	0.57	236.6	5.9×10^6	0.29
971009	Crushed ice	Broken ice	930.	23.1	0.54	195.	4.3×10^6	0.97
971010	Crushed ice	Broken ice	900.	22.1	0.33	235.0	6.2×10^6	0.33
971011	Solid ice	Aluminum	1597.	3.06	0.90	182.5	3.0×10^5	0.19
971012	Solid ice	Aluminum	1680.	3.06	0.95	135.0	1.6×10^5	0.26
971014	Solid ice	Aluminum	1632.	3.06	0.92	108.0	1.1×10^5	0.51
971016	Chipped ice	Aluminum	794.	3.06	0.45	136.7	3.6×10^5	0.17
971017	Chipped ice	Aluminum	751.	3.06	0.43	111.7	2.5×10^5	0.56
971018	Chipped ice	Aluminum	948.	3.06	0.54	80.0	1.0×10^5	0.79
971019	Chipped ice	Aluminum	862.	3.06	0.49	308.3	1.7×10^6	0.02
971020	Pellet ice	Aluminum	1021.	3.06	0.58	304.0	1.4×10^6	0.05
971021	Crushed ice	Broken ice	418.	24.5	0.66	73.0	1.5×10^6	0.59
971022	Crushed ice	Solid ice	360.	14.4	0.60	107	2.1×10^6	0.12
971023	Crushed ice	Solid ice	417.	13.4	0.63	105.0	1.7×10^6	0.21
971024	Solid ice	Broken ice	1637.	13.6	0.92	110.0	4.7×10^5	1.00
971025	Solid ice	Solid ice	1635.	12.5	0.92	117.0	5.1×10^5	0.59

EXPERIMENT PROCEDURES

We conducted a series of impact experiments between September 28 and October 8, 1997, using the NASA Ames Vertical Gun Range (AVGR). Data were obtained for 20 low-velocity (ranging from 73 to 308 m/s) airgun shots, using porous (30–45%) and homogeneous ice spheres as targets. We used a variety of projectiles—aluminum, fractured-ice, and solid ice—to see how the type of impactor affects the collisional outcome in the low-velocity regime. Table I summarizes our collisional experiments.

Targets and projectiles for this experiment run were prepared in a cold room (kept at 5°F) near the impact chamber. Prior to impact, targets were suspended in a large ($\sim 2 \times 2 \times 2$ m) vacuum chamber, which is evacuated to a pressure of about 10 mbars for the impact event. Targets were shot at ambient temperature within 10 min. of being removed from the cold room. The impact chamber floors and walls were padded to protect against secondary fragmentation of the ejecta. Three high-speed (400 frames per second) Milliken cameras were positioned at viewing windows at the side and top of the chamber, perpendicular to the direction of the incoming projectile. A NAC video camera running at 1000 frames per second gave us a real-time evaluation of our shots, and provided a quick measurement of the projectile impact speed. All fragments with a mass greater than 0.5 g were collected and weighed to determine a fragment mass (size) distribution for each of the shots. Smaller fragments melted almost immediately, and could not be collected. The percentage of the target mass recovered and measured for each shot was generally from 80–98%. In addition to the size distribution, a mass-velocity distribution for the ejecta will also be determined by measuring fragment speeds from the filmed records of the experiments. This will be the subject of a future paper.

Target Structure

We used both solid ice and porous ice targets in our program. Porous ice targets have not been used in previous experimental programs, although a number of impact experiments have been carried out using solid ice targets (e.g., Lange and Ahrens 1981, Cintala *et al*. 1985, Kawakami *et al*. 1983) with primarily nonice projectiles. We included solid ice targets in our study primarily to compare our results with those of other workers, but also to provide direct comparison between impact strengths and size distributions from solid and porous targets.

For the porous targets, three different structures were fabricated and labeled as follows:

- *Pellet ice* targets (see Fig. 1a) are formed of cylindrical ice pellets each 8 mm in both diameter and length, having a fairly uniform particle-size distribution.
- *Chipped ice* targets were created by molding frozen commercial water-ice chips into a roughly spherical target body. The constituent particles for this target type were less regularly formed than the pellet particles, and although still approximately similar in size and shape, had a somewhat wider spread in initial particle masses. There were almost no small particles in this distribution.

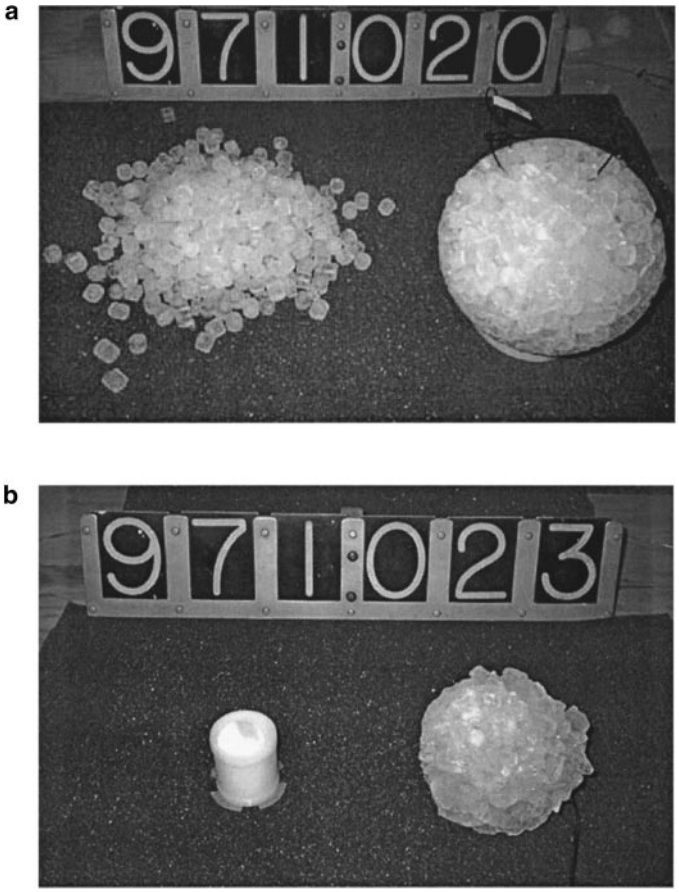

FIG. 1. (a) Finished pellet target and constituent particles. (b) Finished crushed ice target prior to impact.

• *Crushed ice* targets were designed to give the constituent particles a form that mimicked the experimental mass distribution's character: a power-law dependence. This was accomplished by randomly crushing the chipped-ice particles so that small masses were far more numerous than large ones. Therefore, we called this target type "crushed" ice (Fig. 1b).

In all cases the constituent ice particles were formed into targets by allowing them to melt slightly in room temperature air before refreezing them in the target mold. This was necessary in order to produce targets with sufficient mechanical strength for suspension in the target chamber. Porosity for all three target types described above ranged from 30 to 45%.

Projectile Type

For comparison with earlier impact experiments using ice targets, we used aluminum projectiles. However, more realistic collisional experiments for simulated E–K belt collisions should involve icy bodies impacting icy bodies, so we endeavored to shoot ice projectiles with the AVGR airgun. A major experimental problem was keeping the ice projectiles intact through launch. In our first shots, as shown on our film and video records, the projectile broke up in the gun barrel and delivered a spray of fragments to the target. By reducing the air pressure in the gun and ensuring that the projectile was entirely seated within the sabot to reduce shear stresses, we were able to launch intact projectiles. Fortunately, the projectile spray shots could be used to test another variation in collisional condition: the response of our porous targets to a fractured (and presumably much weaker) ice projectile.

EXPERIMENT RESULTS

Fragmentation Mode

Rock targets exhibit several different modes of fragmentation depending on the impact speed of the projectile (Fujiwara *et al*. 1977, Matsui *et al*. 1982, Takagi *et al*. 1984). Core shattering occurs in the high-velocity regime, while in low-velocity impacts, cone-type shattering or longitudinal splitting is commonly observed (see Fujiwara *et al*. 1989 for a more complete discussion of fracturing modes). Neither of these fragmentation modes had been previously observed for homogeneous, ice targets. Instead, these bodies were reported to break into a few large pieces (Fujiwara *et al*. 1989).

Several of our shots (971011, 971012, and 971025) with homogeneous ice spheres displayed what appears to be a combination of cone-type/longitudinal splitting fragmentation mode (see Fig. 2) with fractures originating from the impact point and extending through the target. It is not clear that this fracture pattern has the same origin as cone-type shattering in silicate targets. It should be noted that the largest remnant visible in Fig. 2 is not an antipodal cap as seen by previous researchers (e.g., Giblin *et al*. 1998) in rock fragmentation experiments. The large fracture plane which gave rise to this fragment is in fact parallel with, not perpendicular to, the impact direction.

In the remaining shots, no such distinct fragmentation mode was seen. While the size distribution of many shots resembled that of the three mentioned above (with three to six large fragments dominating the distribution and suggesting a longer fracturing timescale than the initial cratering process), no comparable fragment shapes have been observed. The macroscopically porous nature of the majority of these targets, with a natural preference for fracturing between (rather than across) constituent particles, effectively precluded a classical cone-type/splitting fragmentation mode in many cases. The analysis of the impact films has not yet reached the level of completeness where fragments can be rotated back to their $t = 0$ position and orientations (see Giblin *et al*. 1998). This will be covered in a future paper and will hopefully offer new insights into the fragmentation mode in these porous targets.

Impact Strength

A convenient way to characterize collisional outcomes is through the impact strength of the target material. Impact strength is defined as the total kinetic energy per unit volume of the target needed to produce a largest fragment that contains $\frac{1}{2}$ of

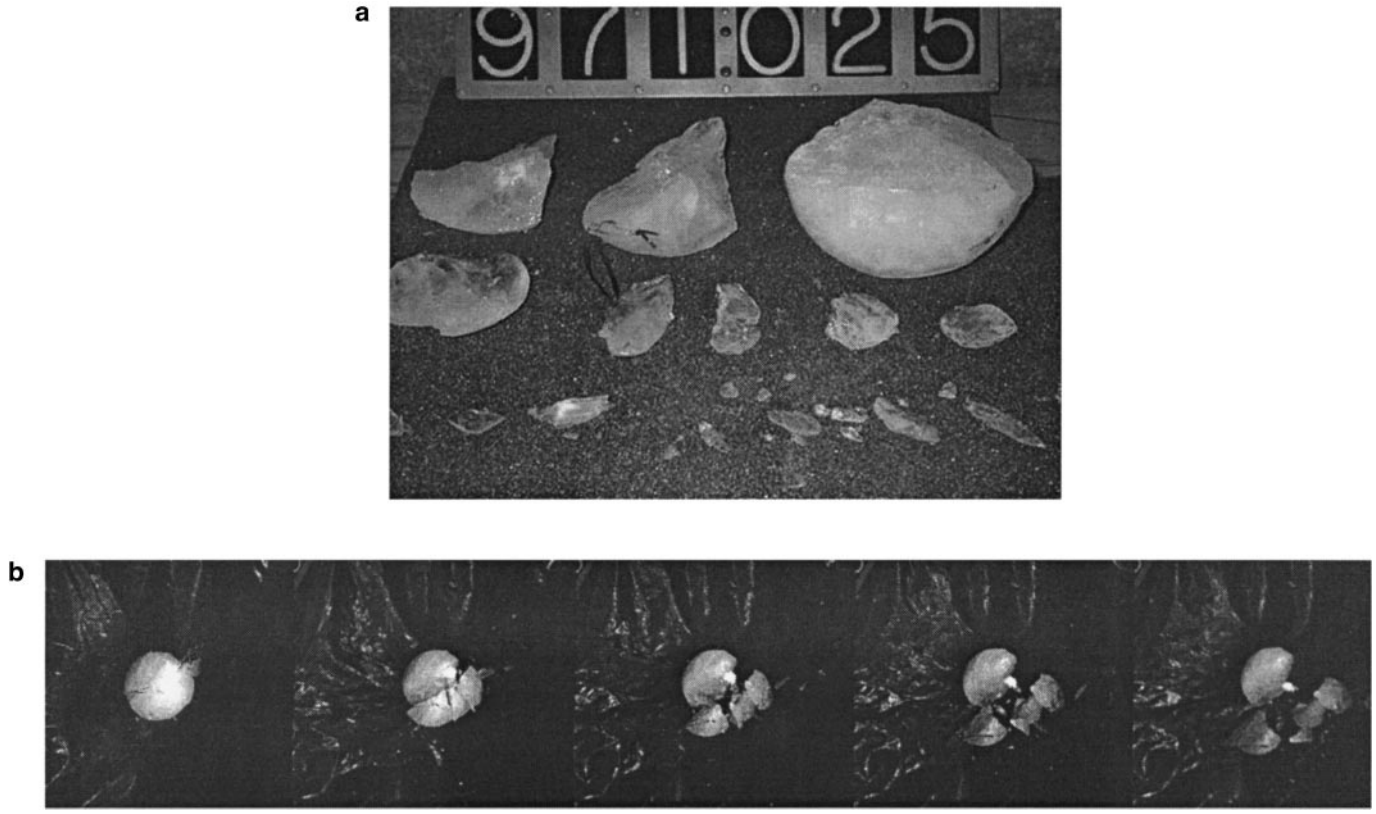

FIG. 2. Cone-type breakup in ice targets. (a) Fragmentation outcome for the solid ice target (shot 971025), showing distinct cone-type fragmentation. (b) Series of impact frames for shot 971025 (solid ice target) confirming cone-shaped fragment formation. Each frame is 0.02 s apart.

the target mass (see Fujiwara *et al*. 1977, Davis and Ryan 1990, Ryan *et al.* 1991). To determine impact strength, we plot the mass of the largest fragment, normalized to the initial target mass (f_1) as a function of the total collisional specific energy Q. Figure 3 shows our results for ice targets of various structures using different projectile types, compared with a wide range of impact experiments using ice, silicate, and metal targets. The results indicate that the degree of fragmentation for ice targets is strongly dependent on the type of projectile used and on the structure of the target. Our results for aluminum projectiles hitting solid ice targets is in good agreement with other experiments using the same target/projectile combination. We determined the impact strength of the solid ice targets hit by aluminum projectiles as about 1×10^5 erg/cm^3, similar to that found by previous workers (Lange and Ahrens 1981, Cintala *et al*. 1985, Kawakami *et al*. 1983).

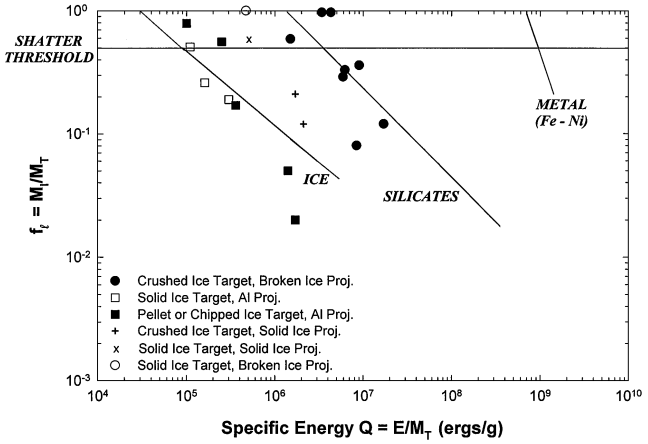

FIG. 3. Results on the mass of the largest fragment (f_1) vs collisional specific energy (Q) for our new results on porous ice targets compared with fits to data from a database of collisional outcomes for ice, silicates, and cooled iron meteorite targets.

When a solid ice target was hit with an ice projectile, either solid or broken, there was much less damage than when an Al projectile was used, implying a higher impact strength for this combination (see Fig. 3). Our data also show that the porous ice targets behave collisionally as if they were as strong as silicates when hit with the fractured projectiles (Fig. 3, solid circles). Porous targets hit by solid ice projectiles are intermediate to the above two cases (Fig. 3). Energy is apparently well dissipated by the void spaces within the target, such that these fragile, porous ice structures are relatively strong in collision. Ryan *et al*. (1991) also found this to be true for porous, preshattered rock targets. Thus, one of the more interesting results of this study is that even though the very porous ice targets have a static material strength well below that for solid ice, they behave

collisionally just as strongly as solid ice. So it would appear that if EKOs are porous (at least, on a macroscopic scale as in our experiments), they are not necessarily collisionally weak. A significant result from our data is that there is systematically less collisional damage to the icy targets at the same specific energy as the projectile type varies from aluminum to solid ice to fractured ice. This suggests a major difference between the low impact velocity shots that characterize the E–K belt and the high velocities that are found in the asteroid belt. In the latter case, the so-called point source approximation holds, where the details of the impactor (size, density, speed) are relatively unimportant to the collisional outcome. The coupling parameter (Housen and Holsapple 1990), which follows from the point source approximation, has been shown to hold for impact speeds greater than a few kilometers per second. When a solid or porous ice target is hit with a solid ice projectile, its impact strength increases to about 5×10^5 erg/cm^3, a factor of 5 larger than that found when using aluminum projectiles. When a porous target is hit with fractured ice its apparent impact strength approaches that found for rock, $\sim 2 \times 10^6$ erg/cm^3.

A contributing factor in these results may be related to work done previously on collisional energy partitioning between target and projectile at low velocities. Ryan and Davis (1991) noted that if the target and projectile have the same material strength, the incoming energy is partitioned equally between them. However, as the projectile strength increases relative to that of the target, an increasing fraction of the collisional energy goes into target breakup, approaching 90% for extreme strength differences. In effect, the target responds as if it had a lower than "normal" impact strength. One possible explanation for this behavior is the variable depth of penetration of the projectile for the different cases. A weak object will deposit its collisional energy at a target depth shallower than that of a stronger projectile, resulting in less efficient energy coupling, and less overall fragmentation. Based on this, if we assume that there has not been significant heating or differentiation in the E–K Belt, the most applicable impact strength for the low-velocity E–K belt collisions is likely to be that derived from similar target/projectile materials impacting each other. The laboratory data from this analysis indicate that a value for impact strength $> 5 \times 10^5$ erg/cm^3 is appropriate for porous ice targets impacted with porous ice projectiles.

Mass Distributions

Our porous targets were constructed using relatively strong chunks of ice of varying sizes. A basic question in our program is: What is the relationship between the pre- and post-impact size distributions? One possibility is that energetic collisions reduce the target structure back to the original particles from which the body was originally constructed. Figure 4 compares the mass distribution of the initial particles with the size distribution of fragments from shots 971019 and 971020. It is clear from this figure that while the size distribution for the constituent particles influences the ejecta size distribution, it also contains many particles both larger and smaller than the original building blocks.

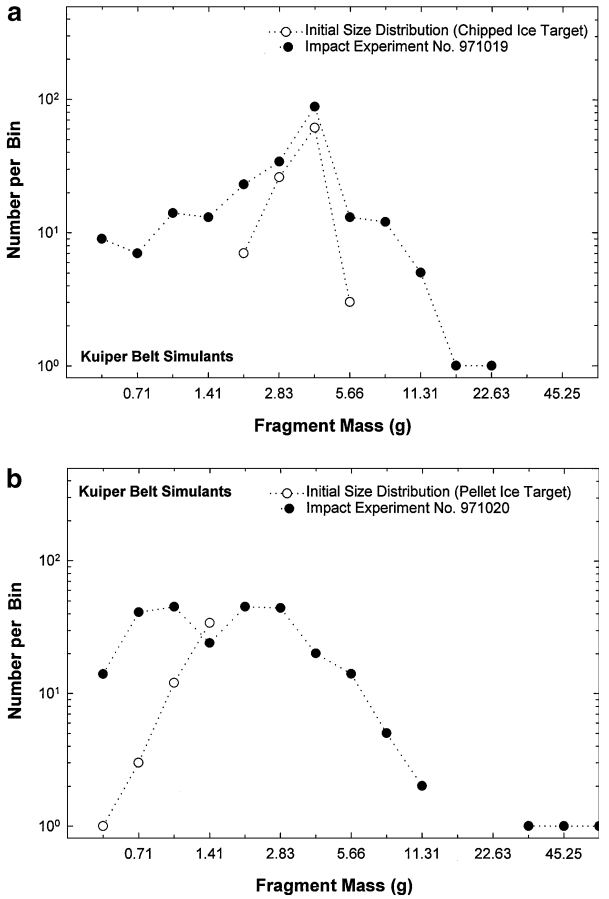

FIG. 4. A comparison of the initial and fragmental size distribution for two types of porous targets. Shown are mass distributions for the constituent particles used in (a) shots 971019 (chipped ice target aluminum projectile at 308 m/s) and (b) 971020 (pellet target, aluminum projectile at 304 m/s).

Bearing in mind our fabrication technique of bonding the particles together by freezing, it is not surprising that there should be members of the fragment size distribution that are aggregates of the original blocks. Even though we tried to make the bonds as weak as possible consistent with having the target stay together before the shot, clearly the bonds were strong enough to resist disruption by the impact process. So we cannot attribute the number of large fragments to any impact process. However, this would not explain the addition of small fragments as seen here (indeed, it works against any small fragments)—so the comminution of initial particles into small fragments must be a result of collisional fragmentation.

The fragment size distributions shown in Fig. 4 exhibit a feature found in other impact experiments (e.g., Fujiwara *et al*. 1977; Capaccioni *et al*. 1984, 1986), namely a two-segment power-law representation. However, the physical basis for the presence of a "knee" is probably quite different in the experiments discussed here. Here, the change in slope indicates a memory of the constituent particle size distribution rather than any difference in fragmentation timescale (e.g., initial cratering versus longer term macroscopic fracturing) as suggested by the

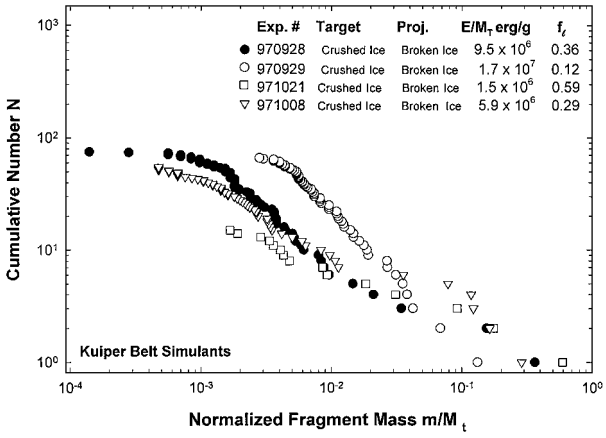

FIG. 5. Cumulative mass distributions for four shots, all of which had a crushed ice target and a broken ice projectile, but having different Q values.

authors mentioned above. The influence of this initial particle distribution is seen where the inflection point for the post-impact fragment masses occurs at the same mass as in the initial particle distribution. A similar result has been found by Durda and Flynn (199) in their experiments on porphyritic olivine basalt targets, where a knee is seen in the size distribution at a mass corresponding to the olivine phenochrysts in the basalt.

In Fig. 5, target/projectile material combinations are fixed, with a similar projectile material impacting a similar target material. We see that the fragmentation trends are directly related to the collisional energy: f_1 gets smaller when energy is increased, and the steepness of the mass distribution slope increases with increasing f_1. However, this apparently simple relationship may have a more complex dependence upon fragmentation geometry. This issue is discussed by Paolicchi *et al*. (1996) and will be covered in a future paper by us.

Figure 6 shows the wide range of collisional outcomes that result when having different projectile/target combinations at the same collisional specific energy Q. Results show no similarities to one another, confirming that fragmentation outcome is not simply governed by the energy of impact, but is more complexly related to the material properties of the bodies involved.

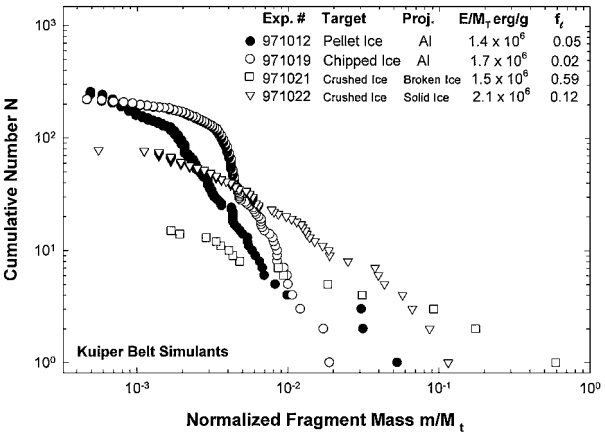

FIG. 6. Cumulative mass distributions for like target/projectile materials and different target/projectile materials, but all at about the same collisional specific energy.

CONCLUSIONS

When ice projectiles are used to shatter ice targets at low impact speeds (hundreds of meters per second), the impact strength is found to be variable, depending on the nature of the target and the type of projectile. For porous bodies impacted by ice projectiles, the impact strength is about 5×10^5 erg/cm^3 for laboratory-sized bodies. This value is higher by a factor of about 5 than the impact strength inferred using aluminum projectiles into solid ice targets.

Weidenschilling (1997) suggested that comets may be porous bodies made up of 100-m-scale building blocks, so one might argue that a building block hitting a larger, "rubble pile structure" might be like broken ice targets struck by a stronger aluminum projectile. However, the Weidenschilling building blocks are also likely to have a weak structure; the nature of any possible lithification mechanism which could significantly increase their mechanical strength has not yet been identified. If there were inherently strong building blocks, and larger bodies are assemblages of such building blocks, then this structure might produce a minimum of Q_d^* at the size of the building bocks. However, we need to understand the physical structure of the building blocks much better before we can assess the implications of such structures.

While some "memory" of the initial (constituent particle) size distribution was retained in a few cases of ice target disruption, this size distribution is modified in the disruption process, as more small particles are formed by fragmentation and larger fragments are possibly formed by agglomeration. Thus, the basic collisional assumptions of studies of the evolution in the E–K belt, namely that EKOs fragment similar to the way that silicate targets fragment, is supported by these laboratory impact experiments. Further work is being carried out using "snowball" targets, a more realistic example of what an EKO might be like.

ACKNOWLEDGMENTS

We appreciate the support of Wayne Logsdon and the Ames Vertical Gun Range staff for their assistance and support in carrying out these experiments. Careful review of this manuscript by D. Durda and P. Paolicchi contributed several insightful comments which led to an improved paper. This project was supported by NASA's Origins program, No. NAG5-4823. This is PSI Contribution 354.

REFERENCES

Capaccioni, F., P. Cerroni, M. Coradini, P. Farinella, E. Flamini, G. Martelli, P. Paolicchi, P. N. Smith, and V. Zappalà 1984. Shapes of asteroids compared with fragments from hypervelocity impact experiments. *Nature* **308**, 832–834.

Capaccioni, F., P. Cerroni, M. Coradini, M. Di Martino, P. Farinella, E. Flamini, G. Martelli, P. Paolicchi, P. N. Smith, A. Woodward, and V. Zappalà 1986. Asteroidal catastrophic collisions simulated by hypervelocity impact experiments. *Icarus* **66**, 487–514.

Cintala, M. J., F. Hörz, S. Smrekar, and F. Cardenas 1985. Impact experiments in H_2O ice, II: Collisional disruption. *Proc. Lunar Planet. Sci. Conf. 16th*, 129–130.

Davis, D. R., and P. Farinella 1997. Collisional evolution of Edgeworth–Kuiper belt objects. *Icarus* **125**, 50–60.

Davis, D. R., and E. V. Ryan 1990. On collisional disruption—Experimental results and scaling laws. *Icarus* **83**, 156–182.

Davis, D. R., S. J. Weidenschilling, P. Farinella, P. Paolicchi, and R. P. Binzel 1989. Asteroid collisional history: Effects on sizes and spins. In *Asteroids II* (R. P. Binzel, T. Gehrels, and M. Matthews, Eds.), pp. 805–826. Univ. of Arizona Press, Tucson.

Durda, D. D., and G. J. Flynn 1999. Experimental study of the impact disruption of a porous inhomogeneous target. *Icarus* **142**, 46–65.

Farinella, P., and D. R. Davis 1996. Short period comets: Primordial bodies or collisional fragments? *Science* **273**, 938–941.

Fujiwara, A., P. Cerroni, D. Davis, E. Ryan, M. Di Martino, K. Holsapple, and K. Housen 1989. Experiments and scaling laws for catastrophic collision. In *Asteroids II* (R. P. Binzel, T. Gehrels, and M. S. Matthews, Eds.), pp. 240–265. Univ. of Arizona Press, Tucson.

Fujiwara, A., G. Kamimoto, and A. Tsukamoto 1977. Destruction of basalt bodies by high-velocity impact. *Icarus* **31**, 277–288.

Giblin, I., G. Martelli, P. Farinella, P. Paolicchi, M. Di Martino, and P. N. Smith 1998. The properties of fragments from catastrophic disruption events. *Icarus* **134**, 77–112.

Holsapple, K. A. 1993. The scaling of impact processes in planetary sciences. *Ann. Rev. Earth Planet. Sci.* **21**, 333–374.

Housen, K., and K. Holsapple 1990. On the fragmentation of asteroids and planetary satellites. *Icarus* **84**, 226–253.

Iijima, Y., M. Kato, M. Arakawa, N. Maeno, A. Fujimura, and H. Mizutani 1995. Cratering experiments on ice: Dependence of crater formation on projectile materials and scaling parameter. *Geophys. Res. Lett.* **22**, 2005–2008.

Jewitt, D., and J. X. Luu 1993. Discovery of the candidate Kuiper belt object 1992 QB_1. *Nature* **362**, 730–732.

Kawakami, S., H. Mizutani, Y. Takagi, M. Kato, and M. Kumazawa 1983. Impact experiments on ice. *J. Geophys. Res.* **88**, 5806–5814.

Lange, A., and T. J. Ahrens 1981. Fragmentation of ice by low-velocity impact. *Proc. Lunar Planet. Sci. Conf. 12th*, 1667–1668.

Marzari, F., P. Farinella, D. R. Davis, H. Scholl, and A. Campo Bagatin 1997. Collisional evolution of Trojan asteroids. *Icarus* **125**, 39–49.

Matsui, T., T. Waza, K. Kani, and S. Suzuki 1982. Laboratory simulation of planetesimal collisions. *J. Geophys. Res.* **87**, 10,968–10,982.

Paolicchi, P., A. Verlicchi, and A. Cellino 1996. An improved semi-empirical model of catastrophic impact processes. I. Theory and laboratory experiments. *Icarus* **121**, 126–157.

Ryan, E. V., and D. R. Davis 1991. Laboratory impact experiments: Ejecta velocity distributions. *Proc. Lunar Planet. Sci. Conf. 22nd*, 1153–1154.

Ryan, E. V., W. K. Hartmann, and D. R. Davis 1991. Impact experiments 3: Catastrophic fragmentation of aggregate targets and the relation to asteroids. *Icarus* **94**, 283–298.

Stern, S. A. 1995. Collision timescales in the Kuiper disk: Model estimates and their implications. *Astron. J.* **110**, 856–868.

Stern, S. A. 1996. On the collisional environment, accretion time scales, and architecture of the massive, primordial Kuiper belt. *Astron. J.* **112**, 1203–1211.

Stern, S. A., and J. Colwell 1997. Accretion of the Edgeworth–Kuiper belt: Forming 100–1000 km radius bodies at 30 AU and beyond. *Astron. J.* **114**, 841–849.

Takagi, Y., H. Mizutani, and S. Kawakami, S. 1984. Impact fragmentation experiments of basalts and pyrophyllites. *Icarus* **59**, 462–477.

Weidenschilling, S. J. 1997. The origin of comets in the solar nebula: A unified model. *Icarus* **127**, 290–306.